Materials Advances

ROYAL SOCIETY OF CHEMISTRY

PAPER

View Article Online
View Journal

Cite this: DOI: 10.1039/d6ma00016a

Hormone-coated nanocontrast agent promotes ER+ breast cancer cell detection

Ankan Biswas[a] and Manos Gkikas †*[ab]

Breast cancer along with colorectal and lung cancer contribute to ~51% of all female cancers and significantly affect women's health. Breast cancer screening with standard medical imaging techniques such as ultrasound, MRI, digital mammography (M; low-energy X-rays), contrast-enhanced mammography (CEM), and X-ray computed tomography (CT; high-energy X-rays) can reduce mortality rates by 20%. High specificity and sensitivity are thus crucial in breast cancer screening. In cases where breast cancer cannot be identified, such as cases of dense breast tumors, CEM is used. However, all the FDA-approved M/CT contrast probes are non-specific blood pool agents that target tumors passively, clear quickly, require high doses, and can lead to side effects. Engineering ligand-specific nanoparticles (NPs) as molecular imaging diagnostic probes that can selectively recognize hormone receptors of breast cancer cells, which account for 70–80% of breast cancer cases, and internalize them, could allow for early identification of tumors/micro-tumors at low metal amounts, lower the imaging sensitivity detection limits, and reduce side effects related to non-specificity (non-targeted probes). Herein, we report on estrogen receptor (ER)-targeting NPs of ~4 nm that can selectively bind and internalize to ER+ breast cancer cells, and dually as fluorescence or M/CT contrast probes, amplifying the signal at the targeting site due to affinity-empowered NP localization within cells. NP preparation, small molecule synthesis, bioconjugation, material characterization, NP/cell internalization and binding studies, as well as micro-CT analysis are described in detail and compared with controls. This is the first study to our knowledge to report hormone-coated NPs as a new M/CT contrast agent for breast cancer screening.

Received 5th January 2026,
Accepted 14th March 2026

DOI: 10.1039/d6ma00016a

rsc.li/materials-advances

Introduction

According to the American Cancer Society, colorectal, lung, and breast cancers contribute to ~51% of all gynecologic cancers, significantly affecting women's health.[1–3] Breast cancer is the most common cancer in women, ranked 6th in terms of cancer-related mortality.[4] Each year, around half a million people are diagnosed with breast cancer and approximately 1 in 5 women affected die,[5] and this number is expected to increase by 39% in 2040. Breast cancer screening using mammography (mainly), CT, or other imaging techniques, can reduce the mortality rates by 20%.[6] In cases where breast tumors cannot be identified, CEM is used.[7] However, all the FDA-approved M/CT contrast probes are non-specific blood pool agents that target tumors passively (enabling poor tumor-to-background contrast), clear quickly, require high doses, and can lead to side effects. Engineering M/CT nanoprobes that can recognize specific hormonal breast cancer cell receptors such as progesterone receptors (PRs) or ERs, which account for 70–80% of breast cancer cases,[8] and internalize them could allow for early identification of tumors/micro-tumors at lower metal amounts than non-targeted nanoprobes, reduce the imaging sensitivity detection limits, and minimize side effects related to non-specific administration.

High levels of female hormones such as progesterone and estradiol in women are strongly connected with breast cancer.[9] β-Estradiol (E2) is an estrogen steroid hormone that is mainly secreted by the ovaries. It can be either found free or loosely bound to albumin (in both cases it is bioavailable and is rapidly extracted by tissues) or tightly bound to sex hormone bound globulin, where it is difficult to diffuse into cells/tissues.[10] Women have 30–400 pg estradiol per mL in their blood (pre-menopausal), while men have 10–50 pg per mL.[11] E2 can be administered pharmaceutically to enhance puberty maturation in cases of hormone deficiency in adults, as an oral contraceptive, for managing amenorrhea, or as a biomarker to examine the development of the ovary follicles prior to *in vitro* fertilization.[12,13] However, E2 plays a crucial role in increasing the risk of ovarian, prostate, and breast cancers.[9,14]

[a] *University of Massachusetts Lowell, Department of Chemistry, Lowell, Massachusetts 01854, USA*
[b] *Northeastern University, Department of Pharmaceutical Sciences, Boston, MA 02115, USA. E-mail: e.gkikas@northeastern.edu*
† Present address: Department of Pharmaceutical Sciences, Northeastern University, Boston, Massachusetts 02115, USA.

ERs are protein receptors that bind β-estradiol and are found in breasts, ovaries, uterus, brain, and even in bones, and among others, regulate sex differentiation. They divide into transmembrane ERs[15] (G protein-coupled receptors) and cytoplasmic ERs[16] (with subtypes ERα and ERβ) which bind E2 and transfer/translocate the hormone to the nucleus, where it binds with DNA and activates transcriptional processes, resulting in gene expression.[17] The two cytoplasmic ER subtypes are located in different tissues in normal humans and animals.[18–21] ERβ is the dominate subtype in the ovaries and in specific regions of the brain (82% and 13% respectively have been found in the ovaries and in all areas of the brain in female rats[21]), while ERα predominately exists in reproductive tissues such as the uterus and in breasts (29% and 26% ERα have been respectively found in the uterus and in the mammary glands of female rats[21]). In the case of breast cancer though, ERα is overexpressed,[22–25] and is found in ∼70–75% of breast cancers.[26]

ERs have been used as an appealing pharmaceutical target for a wide variety of diseases, such as in hormone therapy and breast cancer.[27,28] As an example, estradiol esters (E2 esters) have been approved by the FDA as estradiol pro-drugs. These usually have a short hydrophobic tail[29] or a long-chain fatty acid conjugated to the $C_{17\beta}$–OH group, and can enhance the resistance to the first-pass metabolism as well as improve the E2 bioavailability by gradual release (ester bond degradation) into the bloodstream. While the provided hydrophobic shield of E2 conjugates (estradiol is fat-soluble) protects the hormone, hydrophobic E2 esters have poor access to ERs,[30] and show estrogenic activity only after hydrolysis by esterases. In contrast, hydrophilic E2 conjugates[31–35] may have a higher binding affinity to ERs compared to hydrophobic esters due to the hydration sheath that allows the hormone to come in closer proximity with the binding pocket.

E2 binds to ERα mainly through H-bonding and π–π stacking interactions. Published crystallographic studies by the group of Singler show that the aromatic ring of E2 is involved in π–π stacking interactions with Phe-404 of the ERα.[36] In addition, the aromatic –OH and the aliphatic 17C–OH of E2 donate respectively in H-bonding to Glu-353 and to His-524 of ERα,[36] while the O atom of the aromatic –OH associates with H-bonding to a water molecule residue located between Arg-394 and Glu-353. With reported amounts in the range of $2600 < x < 90\,000$ ERs per cell in ER+ MCF-7 breast cancer cells,[37–39] diagnostic NPs that can hone in on overexpressed ERs of breast cancer cells and amplify the signal seem a very promising and orthogonally-targeted approach to detect breast tumors. By employing this molecular recognition strategy, we aim to fill an existing gap related to the absence of breast-cancer specific M/CT contrast agents that can actively target ER tumors (metallic-NPs absorb X-rays). Currently used iodinated agents are blood pool agents that provide X-ray signals through passive targeting of breast cancer cells, can clear quickly from the body, and lack specificity, resulting in unwanted distribution to different organs. Since mammography is used much more frequently than MRI in hospital settings, developing an ER-targeted probe could be significantly useful for CEM and breast cancer CT diagnosis.

Herein, we report the preparation of estrogen-coated PEGylated AuNPs as a fluorescence and M/CT contrast agent for ER+ breast cancer screening, using two different approaches: (i) a direct E2 conjugation, preparing E2-NPs, and (ii) conjugation through an oligo(ethylene glycol) derivative of E2 (EE2) which enables both –OH groups of the hormone to be free for interaction with the ER binding pocket, yielding EE2-NPs. Both ER-targeting NPs were tested for internalization (confocal fluorescence microscopy) and binding affinity (flow cytometry) with ER+ human MCF-7 breast cancer cells that naturally show overexpression of ERs, and compared with uncoated-NPs, PBS, and a triple negative breast cancer (TNBC) line. A potential internalization mechanism of E2-coated PEGylated AuNPs to ER+ cells is also proposed. Synthetic NP preparation, small molecules synthesis, bioconjugation, material characterization, NP/cell internalization studies, NP/cell binding studies, and micro-CT analysis are described in detail. This is the first study, to our knowledge, that reports hormone-coated NPs as targeting M/CT contrast agents for ER+ breast cancer screening.

Results and discussion

Synthesis of HOOC-PEG-coated gold nanoparticles (HOOC-PEG-AuNPs)

A matrix-free (“one component”[40–42]) hydrophilic contrast probe precursor, HOOC-PEG-AuNPs, was synthesized (Scheme 1) by ligand exchange of 3.7 ± 0.6 nm C12-S-AuNPs (∼11.7 ± 0.3 wt% dodecanethiol incorporation by TGA: thermogravimetric analysis; decomposition temperature: T_d = 301 ± 5 °C; Fig. S1 and S2) with excess HOOC-PEG-SH (PEG had a 96.6 ± 0.2 wt% loss with T_d = 416 ± 1 °C; TGA in Fig. S3) followed by precipitation in hexane to remove liberated dodecanethiol. High speed centrifugation (fractionation) was then used to remove unbound HOOC-PEG-SH, since free polymeric chains have been found to co-exist with polymer-coated NP in previous studies,[40–42] even after extensive dialysis. PEG as a coating favors solubility/dispersibility due to hydration of the NP core, reduces non-specific protein adsorption, provides stealth properties in the bloodstream, and enhances the biocompatibility and half-life of conjugated materials.[43,44] TGA was used to determine the wt% ratio of the coated polymer before and after high-speed fractionation. The crude material, HOOC-PEG-AuNPs, showed a 75.3 ± 0.3 wt% total loss (Fig. S4). Unbound HOOC-PEG-SH chains were then removed *via* high-speed centrifugation,[40] leading to purified HOOC-PEG-AuNPs with two weight losses. One with 9.1 ± 0.2 wt% loss (T_d = 278 ± 3 °C) due to the decomposition of the remaining C12-SH, and another one between 270 and 520 °C with 25.7 ± 1.2 wt% loss (T_d = 411 ± 1 °C) due to the decomposition of NP-bound PEG-SH (Fig. 1a; TGAs are shown analytically in Fig. S5). This allowed for 65.2 wt% Au to remain in the NP. The metal wt% in a nanomaterial is crucial in X-ray absorption methods (mammography and CT), since the higher the number, the stronger the NP-provided contrast. This, however, has a limit

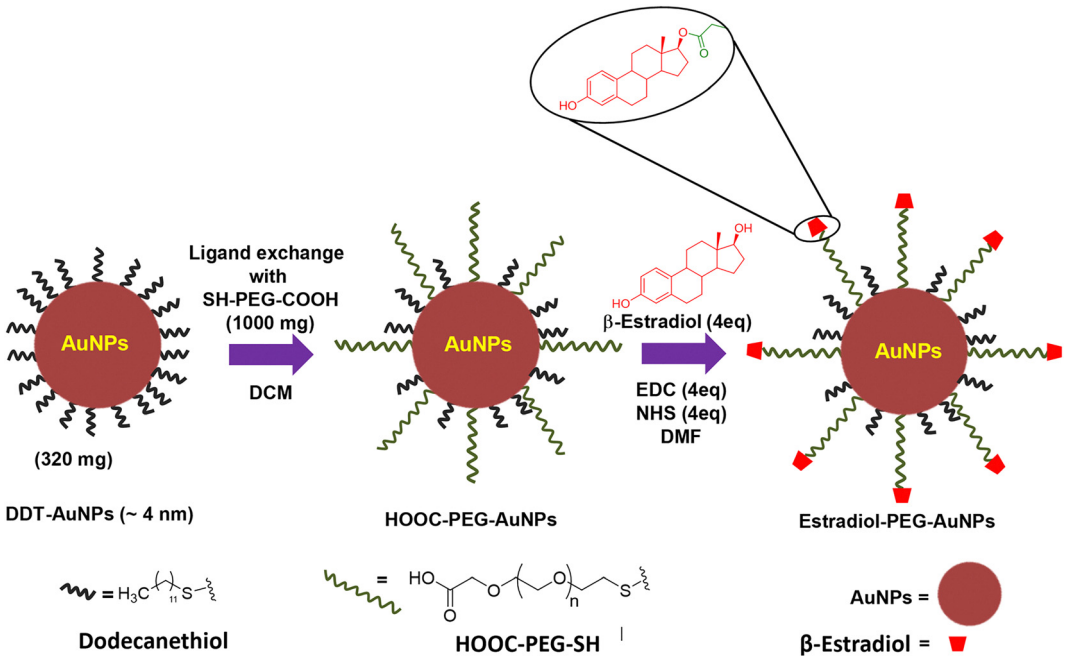

Scheme 1 Preparation of E2-PEG-AuNPs as an ER+-specific M/CT contrast agent.

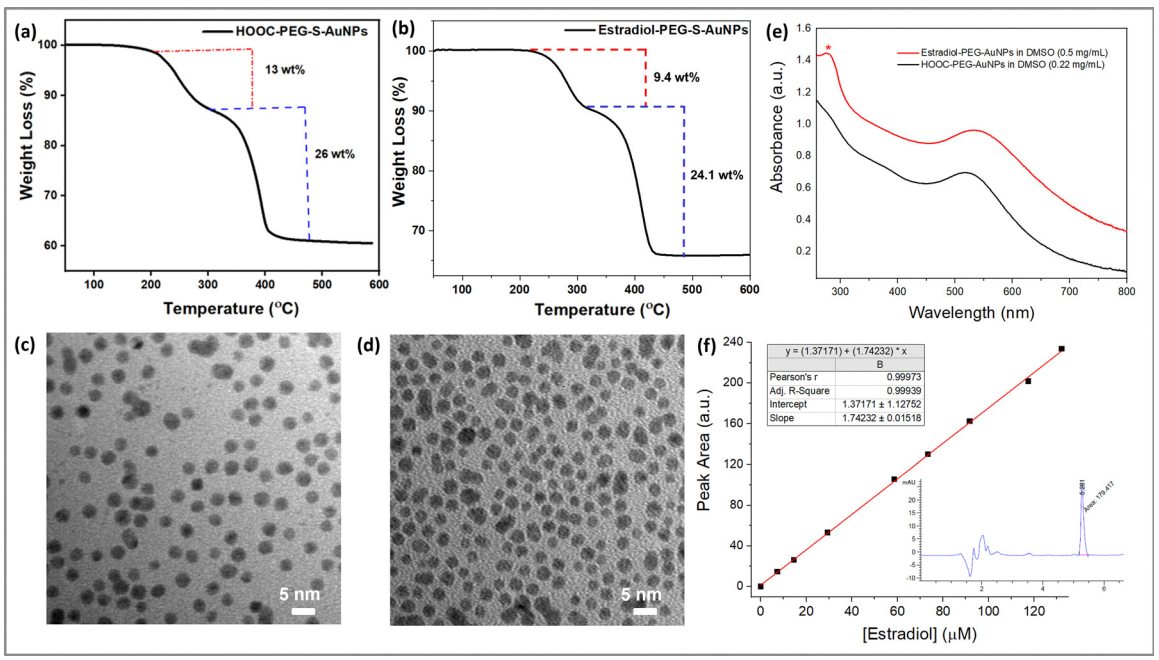

Fig. 1 (a) TGA curve of HOOC-PEG-AuNPs and (b) E2-PEG-AuNPs. TEM images of (c) HOOC-PEG-AuNPs and (d) E2-PEG-AuNPs; (e) UV-vis spectra of the two nanoprobes at 0.5 mg mL^{-1} and 0.22 mg mL^{-1} in DMSO. The estradiol peak at 280 nm is shown with an asterisk; (f) linear fitting of the HPLC peak of E2 between 0 and 132 μM in DMSO. In the inset, the HPLC spectrum of NP-hydrolyzed E2 is shown.

since soft matter (small molecule or polymer) is required to be conjugated to a NP to provide hydrophilicity and hinder possible NP precipitation. Unlike the hydrophobic C12-S-AuNPs which are dispersible in toluene, HOOC-PEG-AuNPs are highly soluble in water, evidenced by reversing the water/toluene phase post extraction. Our studies indicate the significance of the removal of PEG chains using high-speed centrifugation for drug delivery devices, as opposed to dialysis, which can lead to incorrect biodistribution studies.

Synthesis of estradiol-coated PEG-gold nanoparticles (E2-PEG-AuNPs)

Matrix-free HOOC-PEG-AuNPs were subsequently conjugated with β-estradiol in DCM *via* DCC/DMAP-catalyzed ester

coupling, as shown in Scheme 1, followed by dialysis over 50% water–50% MeOH to remove uncoated hormone (which is not soluble in water, but is soluble in DMF, DSMO, and MeOH), then with 75% water–25% MeOH, and finally over water and lyophilized. Purified, E2-PEG-AuNPs showed two weight losses. One with a 9.4 ± 0.3 wt% loss (T_d = 281 ± 1 °C) due to the decomposition of the remaining C12-SH, and another one with a weight loss of 24.1 ± 1.4 wt% (T_d = 411 ± 1 °C) due to the decomposition of NP-bound PEG-E2 (Fig. 1b; shown analytically in Fig. S6). The absence of free estradiol in the NPs was confirmed by thin layer chromatography (TLC in Fig. S7). The NPs' core size was estimated by TEM from different squares of the grid. The average particle size of the HOOC-PEG-AuNPs was found to be 3.2 ± 0.2 nm (Fig. 1c; shown analytically in Fig. S8), while that of the E2-PEG-AuNPs was 3.9 ± 0.7 nm (Fig. 1d; shown analytically in Fig. S9, along with the size distribution), which is slightly higher probably due to the less hydrophilic nature of the steroidal hormone. The NP size in solution was examined by UV-vis spectroscopy. HOOC-PEG-AuNPs showed a surface plasmon resonance (SPR) band at 520 nm, whereas estradiol-PEG-AuNPs had an SPR band at 535 nm (Fig. 1e). The latter, in addition, had an absorption peak at 280 nm due to the coated estradiol. To quantify the NP-bound hormone, E2-PEG-AuNPs were treated with 1 M NaOH overnight to hydrolyze the ester bond. After water evaporation, the solid was dispersed in ethanol, vortexed and centrifuged to isolate the supernatant which contained the ethanol-soluble estradiol (solid NPs remained in the pellet). The hormone was then quantified in DMSO after solvent evaporation, dissolution, and filtration since it has a higher absorption coefficient in that solvent. It was found that 4 mg of NPs per mL contained 105 μM of E2, or 26 nmol E2 per mg NP (Fig. 1f). In contrast, no estradiol peak was found by HPLC for the hydrolyzed HOOC-PEG-AuNPs (Fig. S10).

Internalization studies of E2-PEG-AuNPs with ER+ MCF-7 breast cancer cells

ER+ MCF-7 human breast cancer cells were cultured in Eagle's minimum essential medium (EMEM) supplemented with 10% fetal bovine serum (FBS) at 37 °C with 5% CO_2 at a density of 1–2 × 10^5 cells per mL, and then incubated with E2-PEG-AuNPs (at 220 μg Au) for 24 h. Internalization studies to MCF-7 cells were realized using confocal fluorescence microscopy. Since spherical AuNPs are not fluorescent, an amine-terminated Alexa 594-EG_2 derivative was synthesized (the structure is shown in Fig. S11a). The purity of the product was confirmed by LC-MS (Fig. S11). The fluorescent derivative was then conjugated to the remaining PEG-COOH of the NPs that did not react with E2 *via* EDC/NHS coupling, and the fluorescently-labeled NPs were purified with a Sephadex column. Labeled E2-NPs were eluted first, while unreacted Alexa 594-EG_2 dye was eluted after (see the blue color in Fig. S12). TLC showed the absence of the small fluorescence molecule (Fig. S12). Confocal microscopy showed internalization of (Alexa 594-EG_2)/E2-PEG-AuNPs to MCF-7 cells after 24 h incubation, compared to MCF-7 cells incubated with media only (Fig. 2, upper panel), with the

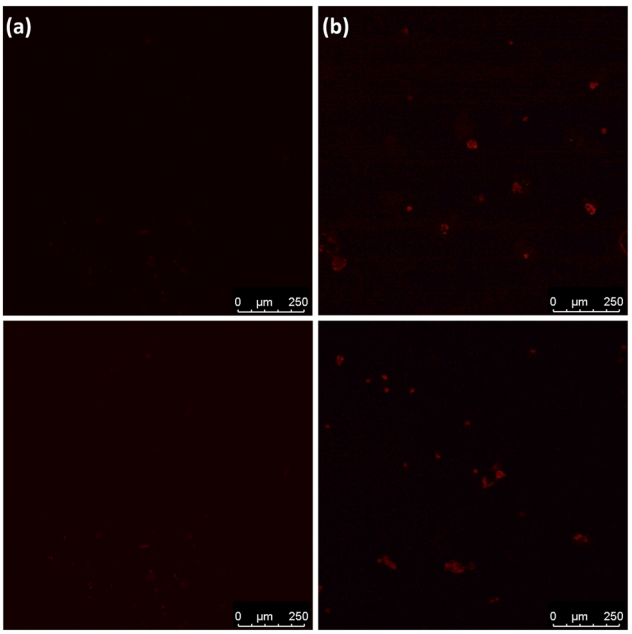

Fig. 2 Confocal fluorescence of ER+ human MCF-7 breast cancer cells incubated with (a) medium only and (b) (Alexa 594-EG_2)/E2-PEG-AuNPs at 220 μg Au after 24 h (upper panel) and 48 h (lower panel). Laser power was 1% and gain was 694 for all the images.

pseudo-red (ex./em. at 590/617 nm) signal inside the MCF-7 cells. A similar outcome was achieved after 48 h of incubation (Fig. 2b, lower panel). To our knowledge, this is the first time that estrogen-coated NPs have been reported. Mechanism of estradiol-NP internalization: estrogen-NPs most probably internalize within MCF-7 cells *via* binding to transmembrane ERs and passing into the cytoplasm, where they can bind to cytoplasmic ERs and provide strong NP contrast. This could be used to enhance the X-ray contrast within ER+ tumors during M or CT breast cancer screening.

Though the results were impressive, solid E2-NPs showed some difficulty in dispersing in water after 3–4 months storage in the freezer. This could not be improved even *via* bath sonication. This was possibly due to the inherently hydrophobic nature of E2, which can be enhanced post conjugation to NPs since only one of the two –OH is free. This motivated us to better engineer our NPs to favor both hydrophilicity as well as interaction with ER receptors of breast cancer cells.

Synthesis of an –OH free estradiol derivative (E2-EG_4-NH_2)

In order to improve the aqueous dispersibility of estrogen-coated NPs as well as achieve stronger E2 binding to the ER pocket without comprising hydrogen bonding interactions of both –OH groups of estradiol with amino acid donor/acceptor groups of the ER pocket, EE2-AuNPs were prepared. E2-EG_4-NH_2 (EE2-NH_2) that has both –OH groups free was synthesized *via* click reaction between ethynyl estradiol with EG_4-azide (Scheme 2). The product was confirmed by LC-MS and NMR spectroscopy. The LC-MS spectrum of the product (MW = 558 g mol^{-1}) showed a peak at *m*/*z* 559 $[M + H]^+$, while the

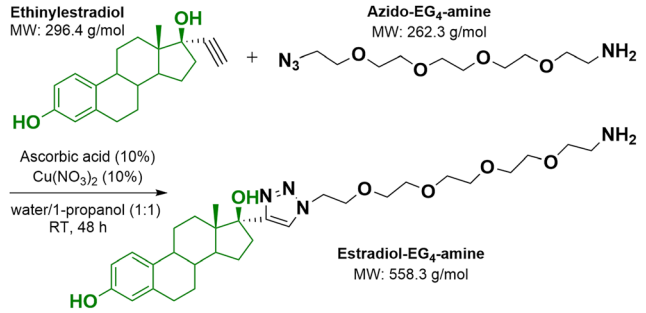

Scheme 2 Synthetic scheme of the click reaction between ethynylestradiol with H_2N-EG_4-azide leading to E2-EG_4-NH_2 with both –OH free.

starting material had a peak at m/z 297 $[M + H]^+$ (Fig. S13). The ^1H NMR of ethynyl estradiol shows the three benzylic hydrogens at 7.09 ppm, 6.55 ppm, and 6.47 ppm. The triple bond –H is shown at 2.89 ppm, while the $–CH_3$ group at 0.85 ppm (Fig. S14). In the ^1H NMR of the product, E2-EG_4-NH_2, the aromatic peaks downshift at 6.99 ppm, 6.55 ppm, and 6.46 ppm (Fig. S15). In addition, a new peak appears at 7.99 ppm, which can be attributed to the triazole ring proton, while the terminal acetylene proton of the reactant (2.89 ppm) disappears (Fig. S15). Other changes include the upshift of the $–CH_3$ group at 1.06 ppm from 0.85 ppm, and the formation of new $–CH_2–$ peaks at 4.59 ppm and 3.91 ppm post conjugation of the EG_4 chain to the triazole ring, compared to the terminal $–CH_2–$ peaks of H_2N-EG_4-azide at 3.52 ppm and 3.38 ppm (Fig. S16).

Synthesis of estradiol-EG_4 coated PEG-gold nanoparticles (EE2-PEG-AuNPs)

A new M/CT contrast probe was synthesized that allowed for both –OH groups of the hormone to be free for interactions, since direct conjugation to one of those could theoretically impact the binding to the ER pocket (though not observed in our confocal study).[36] Starting from a new batch of HOOC-PEG-AuNPs with 34.3 ± 1.0 wt% PEG (TGA in Fig. S17), the synthesized estradiol-EG_4-NH_2 was conjugated *via* EDC/NHS coupling to obtain EE2-PEG-AuNPs with two weight losses; one with a 6.4 ± 0.3 wt% loss (T_d = 272 ± 3 °C) due to the decomposition of the remaining C12-SH, and another one with a weight loss of 35.0 ± 5.5 wt% (T_d = 410 ± 0 °C) due to the decomposition of NP-bound PEG-EE2 (Fig. S18). The amount of Au in the EE2-NP was ~59 wt%, slightly lower than that in the E2-NP (65 wt%). However, unlike the latter, the EE2-NPs had a high aqueous dispersibility after long-term storage in the freezer (tested up to 24 months), which makes them more suitable for commercial purposes. EE2-PEG-AuNPs had a SPR band at 530 nm (Fig. S19), unlike the precursor, HOOC-PEG-AuNPs, which showed a SPR band at 518 nm. The latter, in addition, had a small absorption peak at 280 nm (in MeOH) due to the conjugated EE2. The average particle size of the EE2-PEG-AuNPs was 3.9 ± 0.7 nm (Fig. 3a; the size distribution is provided in Fig. S20), slightly higher compared to the 3.2 ± 0.2 nm of the HOOC-PEG-AuNP precursor. To quantify the NP-bound hormone, EE2-PEG-AuNPs and HOOC-PEG-AuNPs

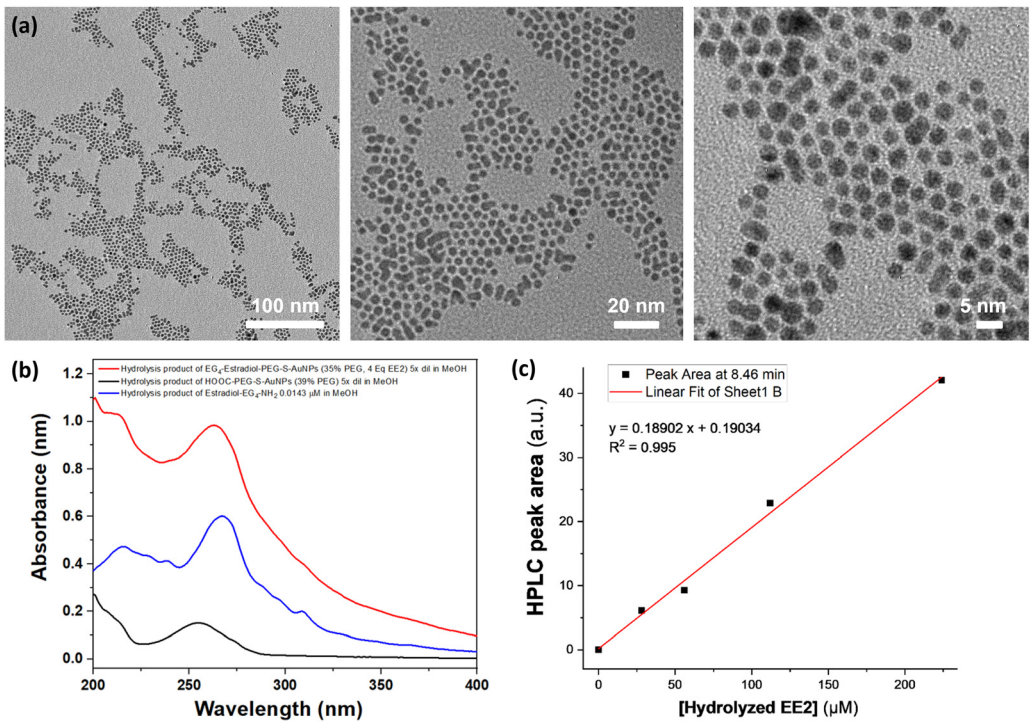

Fig. 3 (a) TEM images of 3.9 ± 0.7 nm EE2-PEG-AuNPs at 0.5 mg mL^{-1} in water. The examined magnitudes (left to right) were 45 000×, 125 000× and 260 000×; (b) UV-vis quantification of acid-hydrolyzed EE2-PEG-AuNPs (red color) and HOOC-PEG-AuNPs (black color) at the same [NP], along with 14 μM E2-EG_4-NH_2 (blue color; standard) at 266 nm. The results showed 21 nmol E2-EG_4 per mg NP. (c) HPLC quantification of the same NP based on the ligand elution peak at 8.46 min. The results showed 11 nmol E2-EG_4 per mg NP and 0 for the negative control.

(control) were hydrolyzed with 6 N HCl at 100 °C overnight. The solid NPs were spun down and the supernatants containing estradiol and/or derivatives (brown color), or the negative control (colorless; from lysed HOOC-PEG-AuNPs) were evaporated, dissolved in 1 mL MeOH and quantified over a calibration curve of hydrolysed E2-EG_4-NH_2 itself (brown color) at 266 nm. It was found that 5 mg of NPs contained 105 nmol of EE2 after subtraction from the negative control (lysed HOOC-PEG-AuNPs), or 21 nmol EE2 per mg NP (Fig. 3b). HPLC was also used as a supplementary technique to quantify EE2-PEG-AuNPs based on a calibration curve of one of the hydrolyzed products of estradiol-EG_4-NH_2. This method revealed 11 nmol EE2 per mg NP (Fig. 3c).

The behavior of EE2-coated NPs was then examined in solution using water and cell media containing BSA. The effect of the cell incubation media on the dynamic NP size was then examined. Dynamic light scattering (DLS) results showed a number-average hydrodynamic size of 36 ± 11 nm for EE2-PEG-AuNPs in water at 0.83 mg mL^{-1} (Fig. S21a), while in DMEM containing 10% FBS the size was 33 ± 10 nm, highlighting the dysopsonic properties of PEG,[45] which hinders proteins like albumin from adsorbing onto the NP surface and increasing the NP size. The larger NP size in DLS (solution size) compared to TEM (core size; dry state) is expected due to the conjugation of PEG which interacts with neighboring polymeric chains in water. A similar increase in size (from TEM to DLS) due to polymer attachment was reported by Cai *et al.*,[46] the group of Badea,[47] as well as by our group.[41] DLS is known to be impacted by NP concentration. We thus examined the NP solution size at 0.33 mg mL^{-1} and 0.83 mg mL^{-1}. At the lower concentration, the DLS results showed a size of 53 ± 2 nm in water, while the NPs in DMEM containing 10% albumin as the dispersant solvent had sizes of 50 ± 7 nm (Fig. S21b). The slightly larger size in dilute solution is attributed to the hydrophobic nature of the NP-conjugated hormone which seems to be more pronounced. At higher NP concentrations, polymer–polymer interactions may suppress this effect.

Binding studies of EE2-PEG-AuNPs to MCF-7 breast cancer cells

Similarly to E2-coated NPs (shown in Fig. 2), EE2-PEG-AuNPs showed internalization within ER+ MCF-7 breast cancer cells (Fig. S22). This, along with their high dispersibility after long storage in the solid state at low temperatures, makes them a strong contrast tool for confocal studies and X-ray imaging. To examine potential binding of EE2-PEG-AuNPs to ER+ MCF-7 human breast cancer cells, the cells were grown at a density of 2×10^5 cells per mL, as described above, and incubated with media only as a control, the uncoated-NPs (HOOC-PEG-AuNPs), and (Alexa 594)/EE2-PEG-AuNPs (scheme at Fig. 4) at 119 μg Au per mL for 20 h, followed by washing of the adherent flask with media to remove any unbound dye. The results showed an absence of binding for PBS and the uncoated-NP (Fig. 4a and c and the polygon black line in Fig. 4b) and strong binding for the fluorescently-labeled EE2-NPs (Fig. 4d and e). The performance of (Alexa 594)/EE2-PEG-AuNPs was also tested using the TNBC line MDA-MB-231. The results showed some binding/fluorescence as a result of non-specific binding (Fig. S23b *vs.* Fig. S23a). However, the intensity of the signal was ~5.6 times weaker (see the histogram values in Fig. S23d) than that of MCF-7 cells, using the same polygon (gating area, Fig. S23c).

The X-ray contrast ability of our EE2-NP was then examined. Micro-CT images of NPs in solution showed 1.43× contrast-enhancement for EE2-PEG-AuNPs *vs.* water (Fig. 5a and b). This value is similar to that of FDA-approved iodinated agents in solution at the same metal concentration (not shown here). It is important to note that the CT signal of NPs accumulated (by ligand–receptor affinity) to tumors, which contain by default less/much less water, is expected to be enhanced (zero or negative CT values are often obtained in tissues with a small amount or no water, *e.g.*, fat tissue; water on the other hand gives CT contrast, as shown in Fig. 5a). Enhancing the M/CT signal within breast cancer cells/tumors using receptor-targeting contrast agents at low metal amounts is highly important. The obtained optical microscope image of ER+ MCF-7 breast cancer cells populated by EE2-NPs attests towards that direction (Fig. 5c).

The top priority in hospital breast cancer screening settings is sensitivity and specificity. Our studies indicate specific and selective NP contrast in ER+ breast cancer cells by using E2-coated NPs. Two methods to conjugate E2 to NPs were described in this paper, followed by internalization and binding (flow cytometry) studies. E2 conjugation to NPs through click chemistry (EE2-coated NPs) where both estradiol –OH groups are free, increases hydrophilicity, and favors stronger binding to the ER pocket (the original drug structure is preserved). It is thus the preferred option between the two estradiol-coated NPs. We envision that our E2-coated NPs could be used as a delivery scaffold to selectively transfer M/CT contrast[41,48–55] to orthotopic xenograft ER+ animal tumor models. A high NP accumulation is expected in the tumor due to the increased specificity, followed by renal clearance due to the small size, while small NP accumulation is anticipated in the liver.

Our long-term goal is the translation of this ER-selective NP agent either as an IV-injectable M/CT contrast material or as a breast-absorbing diagnostic cream. We project that 1/5 to 1/2 less metal will be required to provide X-ray contrast *vs.* currently used I-agents (~30 g of I in a human is equal to 9–10 mg I for a 25–30 g mouse), based on previously published results by our group.[41] This could reduce side effects, yet achieve high contrast in breast tumor cases. Though possible NP accumulation to other tissues in which ERs are normally expressed (uterus, ovaries, and some vasculature) cannot be excluded, the high amounts of ERα in malignant mammary tissues with potential administration of the contrasting nanoprobe in a cream formulation in small metal amounts[41] render these off-target accumulations less probable, and by far less toxic compared to current side effects imposed by a non-targeted administered probe. Overall, the ER-targeted NP would be the preferable contrast agent for CEM due to its specificity (more contrast-to-target with fewer side effects), compared to a regularly-used uncoated M/CT probe. In addition, it will be favored against

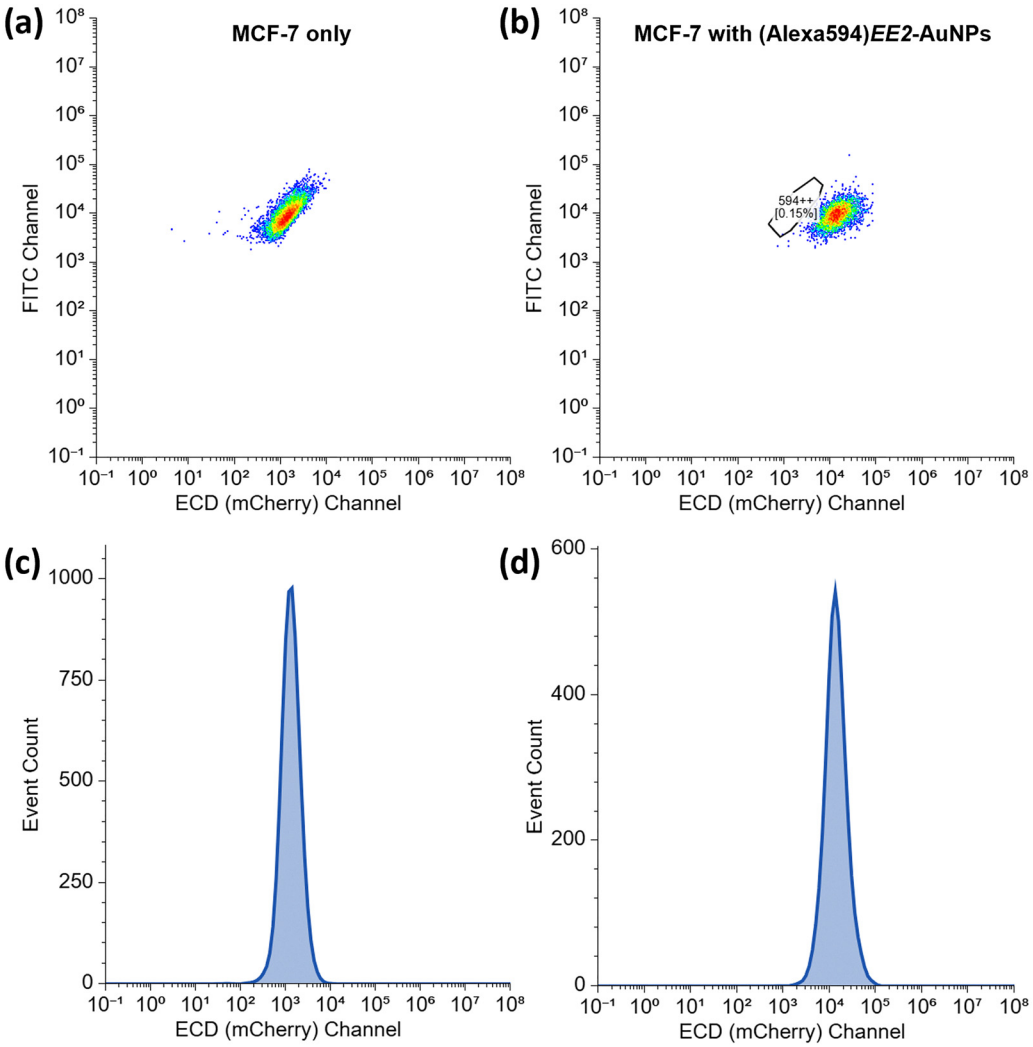

Fig. 4 Schematic of the (Alexa 594)/EE2-PEG-AuNPs; (a)–(d) flow cytometry binding studies of MCF-7 cells incubated with (a and c) medium only, and (b and d) (Alexa 594)/EE2-PEG-AuNPs at 119 μg Au per mL. The polygon black line in (b) indicates the binding of uncoated HOOC-PEG-AuNPs to MCF-7 cells, revealing an absence of binding. The results are shown after the removal of media and washing steps to remove unbound dye. Fluorescence patterns in the mCherry channel (exc./em. 587/610 nm) over the FITC channel (reference; no fluorescence) are shown in (a) and (b), while (c) and (d) represent histograms.

contrast-enhanced MRI in hospital settings, since mammography is much cheaper and the first option for insurance companies. E2-coated nano-contrast M/CT agents could be further coupled with anti-cancer drugs either physically (electrostatic interactions[56–58]) or chemically[59] to develop targeted X-ray/CT theranostic nanoprobes (future direction).

Conclusions

Herein, we report the preparation of estrogen-coated PEG-AuNPs as a fluorescence and X-ray contrast agent for ER+ breast cancer screening. Two different synthetic approaches are described: (i) direct estradiol conjugation, preparing E2-NPs, and (ii) conjugation through an oligo(ethylene glycol) derivative of E2 (EE2), which enables both –OH groups of the hormone to be free for interactions with the ER binding pocket, yielding EE2-NPs. Both estrogen-NPs managed to internalize to ER+ human MCF-7 breast cancer cells (confocal fluorescence microscopy) that have a high expression of ERs. A potential internalization mechanism of E2-coated NPs to ER+ cells is proposed. Strong binding affinity of EE2-NPs with ER+ cells (flow cytometry) was additionally shown, compared to uncoated-NPs, PBS, and a TNBC cell line. While both estrogen-coated NPs could provide fluorescent contrast within ER+ cells, the E2-NPs had difficulty dispersing in water after 3–4 months storage in the freezer. EE2-NPs, in contrast, were easily dispersed even after 24 months of storage at low temperature. Enhanced micro-CT contrast was also achieved with the EE2-coated NPs in solution, highlighting the dual contrasting ability of our synthetic nanoprobe (fluorescence and CT). This is the first study, to our knowledge, that reports hormone-coated NPs as a targeting contrast agent for ER+ breast cancer

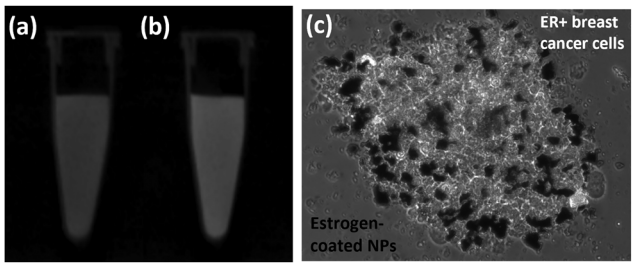

Fig. 5 Micro-CT images of (a) water and (b) EE2-PEG-AuNPs in water showing 1.43× contrast-enhancement in solution; (c) optical microscope image of ER+ MCF-7 breast cancer cell aggregates populated by EE2-PEG-AuNPs.

screening (first line screening). Future research directions will involve evaluating this nanoprobe in a ER+ orthotopic xenograft rodent model, similar to our previous preclinical study in TNBC.

Materials and methods

Materials

Dodecanethiol-functionalized gold nanoparticles were purchased from Nanoprobes Inc. Carboxymethyl-PEG-thiol (HOOC-PEG-SH; 5000 g mol^{-1}) was purchased from Laysan Bio Inc. β-Estradiol was purchased by MD Biochemicals. Ethinylestradiol, ascorbic acid, and azido-EG_4-NH_2 were purchased from TCI Chemicals. MCF-7 and MDA-MB-231 human breast cancer cells (mammary gland), DMEM, and EMEM media were acquired from ATCC. Fetal bovine serum (FBS) and Alexa Fluor™ 594 NHS (succinimidyl ester) were purchased from ThermoFisher.

Synthesis of HOOC-PEG-gold nanoparticles (HOOC-PEG-AuNPs)

PEGylated AuNPs were prepared by ligand exchange of C12-S-AuNPs with excess HOOC-PEG-SH. 1000 mg of HOOC-PEG-SH (0.2 mmol, M_n = 5000 g mol^{-1} per manufacturer) were dissolved in 30 mL DCM and equilibrated at RT. Subsequently, a 20 mL DCM solution of C12-S-AuNPs (320 mg, 89% metal per TGA = 285 mg Au) was added dropwise (the polymer concentration was reduced to 2 wt%), followed by continuous stirring at RT overnight. The solvent was then evaporated, the mixture was dispersed in the minimum amount of DCM (∼2 mL), and precipitated in hexane to remove liberated dodecanethiol. The product (∼1200 mg) was then dispersed in DI water at 10 wt% and centrifuged at 20 000 rpm for 3 h at 8 °C to remove unbound PEG-SH (supernatant), concentrating the HOOC-PEG-AuNP nanocomposite precipitate. The final pellet (∼278 mg) was collected and dried under vacuum overnight at RT. Every step was monitored by TGA. The collected PEG-coated AuNPs were highly soluble in water. Addition of toluene showed clear transfer to the aqueous phase, unlike C12-S-AuNPs.

Preparation of E2-PEG-AuNPs

HOOC-PEG-AuNPs (238.0 mg; 33.3 wt% PEG, ⇒78.6 mg PEG-COOH in Au, ⇒15.75 × 10^{-6} moles since PEG is 5 K) were dispersed in 9.3 mL DMF (4 wt%) and sonicated until well-dispersed. Then, β-estradiol (17.3 mg, 63.0 × 10^{-6} moles, 274.2 g mol^{-1}, 4 eq.) was added as a solid. Subsequently, DCC (6.4 mg, 31.5 × 10^{-6} moles, MW = 206.33 g mol^{-1}, 2 eq.) in 2.7 mL DMF, along with DMAP (0.35 mg, 31.5 × 10^{-7} moles, MW = 122.17 g mol^{-1}, 0.2 eq.) in 0.53 mL DMF (from a concentrated solution) were added and the system was left to react overnight (final [nano] ∼2 wt%). The crude mixture was then dialyzed over 50% water–50% DMF (1 day) to remove the unconjugated hormone, then with 50% water–50% MeOH (2 days), and finally over water (2 days), and lyophilized.

Hydrolysis of E2-PEG-AuNPs/E2 quantification

4 mg of estradiol-PEG-AuNPs were dispersed in 1.6 mL of 1 M NaOH (2.5 mg mL^{-1}) and the solution was stirred overnight. After that, the reaction mixture was neutralized (pH = 7) with 1 M HCl, and the dispersion was evaporated by rotary evaporator (in a vial). The remaining solid was dispersed in 2 mL ethanol (2 mg mL^{-1}) and centrifuged (×3724*g*, 4000 rpm, 1 h, 25 °C) to remove solid particles and obtain the hormone. The collected supernatant was then passed through a 0.22 μm PTFE syringe filter and dried to obtain the hydrolyzed estradiol. The released hormone was dissolved in 1 mL DMSO (4 mg NP mL^{-1}), filtered with a 0.22 μm PTFE syringe filter, and quantified by HPLC using a calibration curve between 0–132 μM estradiol solutions in DMSO. The procedure was repeated twice. A control, HOOC-PEG-AuNPs, was also processed in the same way and quantified as a reference. The samples were also quantified by UV-vis.

Synthesis of Alexa Fluor 594-(ethoxy)ethanamine (Alexa Fluor 594-EG_2-NH_2)

1,2-Bis(2-aminoethoxy)ethane (0.18 mg, 1.21 × 10^{-6} moles, MW = 148.2 g mol^{-1}, 3 eq.) was dissolved in 0.2 mL dry DMSO. Then Alexa Fluor 594 NHS ester (0.33 mg, 2 mM, 0.4 × 10^{-6} moles, MW = 819.9 g mol^{-1}) was dissolved in 0.2 mL dry DMSO and added dropwise. The reaction was left overnight (covered with foil). The product was purified by precipitation in a large volume of diethyl ether to dissolve the excess diamine, and characterized by ESI-MS spectroscopy. Initial reactants were not observed by ESI-MS. ESI-MS *m*/*z* calculated for $C_{42}H_{51}N_4O_{11}S_2$:851.30 $(M + H)^+$; found: 851.0 $(M + H)^+$.

Conjugation of E2-PEG-AuNPs or EE2-PEG-AuNPs with Alexa Fluor 594-EG_2-amine (synthesis of (Alexa 594)/E2-coated NPs)

E2-PEG-AuNPs (10 mg; 24 wt% PEG, ⇒2.4 mg PEG in Au, ⇒4.8 × 10^{-7} moles –COOH since PEG is 5K; assuming all –COOH are reactive) were dissolved in 190 μL DMSO (4 wt%) and sonicated until well-dispersed. Subsequently, 10 μL of a 30 mg mL^{-1} DMSO solution of EDC (0.3 mg, 1.92 × 10^{-6} moles, 155.25 g mol^{-1}, 4 eq.) were added. After 5 min, 10 μL of a 22 mg mL^{-1} DMSO solution of NHS (0.2 mg, 1.92 × 10^{-6} moles, 115.09 g mol^{-1}, 4 eq.) were added. The mixture was sonicated for 2–3 min and was left to react for 20 min. The dispersion (210 μL) was added dropwise to a 290 μL DMSO solution of Alexa Fluor 594-EG_2-amine (0.5 mg, 5.9 × 10^{-7} moles, 850.29 g mol^{-1}, 1.2 eq.), and the reaction was left overnight

(final $C_{nanomaterial}$ ~ 2 wt%, ~20 mg mL^{-1}; 500 μL). The unreacted dye was separated from the labeled-AuNPs using a Sephadex G-25 column, followed by NP fractionation (×3724 *g*, 4000 rpm, 1 h, 25 °C) to remove traces of dye in the collected fraction. The material purity was tested with TLC to confirm the absence of unreacted dye. The same procedure was repeated for Alexa594-labelling of EE2-PEG-AuNPs (35 wt% PEG).

Synthesis of E2-EG$_4$-NH$_2$

118 mg of ethynylestradiol (0.40 mmol, MW = 296.41 g mol^{-1}.), 7.2 mg of ascorbic acid (40 μmol, MW = 176.12 g mol^{-1}, 10 mol%) and 7.6 mg of $Cu(NO_3)_2$ (40 μmol, MW = 187.56 g mol^{-1}, 10 mol%) were added to a mixture of 2 mL water and 2 mL of 1-propanol. After that, 105 mg of azido-EG$_4$-NH$_2$ (0.40 mmol, MW = 262.3 g mol^{-1}, 1 eq.) was added to the reaction mixture. The reaction was carried out for 48 h at room temperature. The solvent was then evaporated, and the greenish mixture was dissolved in 1 mL MeOH and precipitated in a large volume of ethyl acetate to remove excess azido-EG$_4$-NH$_2$. The precipitate was then collected and passed through a silica column to remove the catalyst and obtain a yellow-colored pure product. The elution solvent system was ethyl acetate/MeOH 25 : 75.

Ethynyl estradiol. ^{1}H NMR, (400 MHz, methanol-D4, reference = δ 3.31): δ 7.09 (d, J = 8 Hz, 1H), δ 6.55 (d, J = 8 Hz, 1H), δ 6.47 (s, 1H), δ 2.89 (s, 1H), δ 2.70–2.83 (m, 2H), δ 2.22–2.35 (m, 2H), δ 2.08–2.15 (m, 1H), δ 1.84–2.01 (m, 3H), δ 1.70–1.79 (m, 3H), δ 1.23–1.46 (m, 4H), δ 0.85 (s, 3H). MS (ESI): *m*/*z*: 297.0 ([M + H]$^+$).

EG$_4$-azide. ^{1}H NMR, (400 MHz, methanol-D4, reference = δ 3.31): δ 3.63–3.68 (m, 14H), δ 3.52 (t, J = 4 Hz, 2H), δ 3.38 (t, J = 4 Hz, 2H), δ 2.79 (t, J = 4 Hz, 2H). MS (ESI): *m*/*z*: 263.0 ([M + H]$^+$).

Estradiol-EG$_4$-NH$_2$. ^{1}H NMR, (400 MHz, methanol-D4, reference = δ 3.31): δ 7.88 (s, 1H), δ 6.99 (d, J = 8 Hz, 1H), δ 6.51 (d, J = 8 Hz, 1H), δ 6.47 (s, 1H), δ 4.59 (t, J = 4 Hz, 2H), δ 3.91 (t, J = 4 Hz, 2H), δ 3.71 (t, J = 4 Hz, 2H), δ 3.59–3.67 (m, 14H), δ 3.13 (t, J = 4 Hz, 2H), δ 2.72–2.80 (m, 2H), δ 2.43–2.49 (m, 1H), δ 1.82–2.16 (m, 6H), δ 1.42–1.65 (m, 6H), δ 1.26–1.34 (m, 2H), δ 1.04 (s, 3H), 0.70 (t, J = 4 Hz, 1H). MS (ESI): *m*/*z*: 559.0 ([M + H]$^+$).

Preparation of estradiol-EG$_4$-PEG-AuNPs (EE2-PEG-AuNPs)

HOOC-PEG-AuNPs (100 mg; 35 wt% PEG, ⇒35 mg PEG in Au, ⇒7 × 10^{-6} moles –COOH since PEG is 5K) were dissolved in 2.5 mL DMSO (4 wt%) and sonicated until well-dispersed. Subsequently, EDC (4.3 mg, 28.0 × 10^{-6} moles, 155.25 g mol^{-1}, 4 eq.) was added. After 10 min, NHS (3.2 mg, 28 × 10^{-6} moles, 115.09 g mol^{-1}, 4 eq.) was added. The mixture was sonicated for 5 mins, and left to react for 20 min. Finally, E2-EG4-amine (15.6 mg, 28.0 × 10^{-6} moles, 558.34 g mol^{-1}, 4 eq.) dissolved in 0.5 mL DMSO was added dropwise and the reaction was left overnight. The crude mixture was then dialyzed over 50% water–50% MeOH (2 days) and finally over water (2 days) and lyophilized.

Hydrolysis of EE2-PEG-AuNPs/E2 quantification

5 mg of EE2-PEG-AuNPs or HOOC-PEG-AuNPs were dispersed in 1 mL of 6 N HCl and the reaction mixture was heated at 100 °C overnight. Next, the HCl was evaporated and the remaining solid was dispersed in 1 mL methanol and centrifuged ×2 at 3724*g*, 4,000 rpm, 30 min, 25 °C to remove solid particles and obtain the hydrolyzed product (brown for estradiol-containing NPs and transparent for the negative control). The product was dried, dissolved in 1 mL of fresh MeOH and the UV-vis spectrum was obtained. To build the calibration curve, 1 mg of estradiol-EG$_4$-NH$_2$ (558 mg mmol^{-1}) in 1 mL of 6 N HCl was hydrolyzed under the same conditions and diluted at different concentrations. The methanol-soluble product(s) had a brown color.

Breast cancer cell internalization studies with (Alexa 594)/E2-PEG-AuNPs and (Alexa 594)/EE2-PEG-AuNPs

Human MCF-7 breast cancer cells (breast tissue; mammary gland) were cultured at 37 °C with 5% CO_2 in a 25 cm^2 tissue-culture treated flask in EMEM supplemented with 10% FBS and were then trypsinized at a density of 2 ×10^5 cells per mL. 1 mL of that culture was split into three parts, and 0.33 mL of the cell culture was added to a tissue-culture treated 12-well plate, followed by the addition of 0.67 mL universal growth media (1 mL total volume). After subculturing for 2 days, the medium was decanted, and 1 mL of medium or (Alexa 594)/E2-PEG-AuNPs supplemented in medium at 220 μg Au per mL were added and incubated for 24 and 48 h. To prepare the (Alexa 594)/E2-PEG-AuNPs, 1 mg of material (containing 67 wt% Au) was dispersed in 1 mL medium (667 μg Au per mL), followed by 5 min sonication, and 0.33 mL of that solution were added into the 12-well plates containing equal numbers of MCF-7 cells, followed by addition of medium to reach a volume of 1 mL in total (the metal content was 220 μg Au). After 24 h co-incubation, cells with or without NPs were trypsinized, pelletized, washed twice with PBS to remove unbound NPs, and redispersed in 1 mL fresh media containing 4% paraformaldehyde for 10 min. The cell suspensions were then centrifuged at 1024*g* (1100 rpm) for 5 min to remove unreacted formalin, and the three obtained cell pellets were finally resuspended in 0.2 mL DI water to concentrate cells. A drop of each suspension was added on a glass slide, dried under laminar flow in the biosafety cabinet, and mounted with nail polish in a cover slip. Fluorescence was then measured on a confocal (Leica SP8) laser scanning microscope at 590/617 nm excitation/emission. The same procedure was repeated for (Alexa 594)/EE2-PEG-AuNPs.

Breast cancer cells binding studies with (Alexa 594)/EE2-PEG-AuNPs

ER+ MCF-7 breast cancer cells and TNBC MDA-MB-231 cells were cultured in DMEM medium supplemented with 10% FBS in a 25 cm^2 tissue-culture treated flask for 5–6 days and were then trypsinized. 1 mL of that culture was transferred (at a density of 2.0 × 10^5 cells per mL) to three 12-well plates, followed by 1 mL of media. After two days of subculturing, media were decanted, and 2 mL of fresh media (control), or HOOC-PEG-AuNPs (uncoated-NPs) in media, or (Alexa 594)/EE2-PEG-AuNPs in media at 119 μg Au per mL were added. After 20 h of incubation, media (without and with NPs) were

decanted to remove unbound NPs, cells were washed with media, and trypsinized. Cells were then resuspended in 1 mL fresh DMEM media, mixed well to break any cell clusters, and passed through a 100 μm Falcon® cell strainer. Flow cytometry studies were conducted by using only cell singlets and monitoring the same polygon area of interest (gating) for consistency in all examined samples. Fluorescence was measured on the mCherry channel (ECD; exc./em. 587/610 nm) over the FITC channel (exc./em. 495/519 nm) as a reference. Alexa 594 exhibits 590/617 nm excitation/emission.

Characterization

NMR data were acquired using a JEOL 400 MHz NMR equipped with auto sampling and automatic tuning and matching. LC–MS samples were run on a Shimadzu 8040 Triple Quadrupole LC/MS; 30 μL of unknown sample were injected on a Thermo Fisher ODS C18 Hypersil 4.6 × 60 mm column (3 μm particle size), which was kept at 40 °C temperature. The gradient mobile phase consisted of 0.1 M formic acid in water (solvent A) and 0.1% formic acid in acetonitrile (solvent B), started with 95:5 A/B, increased over 2 minutes to 100% acetonitrile, and held at 100% acetonitrile for 2 minutes, pumped at a 0.5 mL min^{-1} flow rate. Two methanol washings were carried out after each measurement. For TGA analysis, the samples were vacuum-dried overnight at room temperature before the analysis, and measured (in triplicate) on a Mettler Toledo TGA thermal analyzer at a heating rate of 20 °C min^{-1} under N_2 from 50 to 600 °C. UV-vis images were collected on a Thermo Scientific Evolution 60 s between 300 and 700 nm. TEM images were collected on a Philips CM12 electron microscope operated with an acceleration voltage of 120 kV. C12-S-AuNPs were prepared at 0.5 mg mL^{-1} in hexane, while HOOC-PEG-AuNPs and E2-PEG-AuNPs were prepared in water at 0.5 mg mL^{-1}. To estimate core size, more than 300 NPs were measured and analyzed with ImageJ. For HPLC analysis, 20 μL of estradiol standards at 0–132 μM dissolved in DMSO or hydrolyzed NPs at 4 mg mL^{-1} were injected into a Phenomenex Column Prodigy 5 μm 150 × 4.6 mm ODS(2) at a flow rate of 1 mL min^{-1}. A solvent gradient of 40% v/v acetonitrile in water was used, which linearly rose to 100% (v/v) acetonitrile at 10 min. This flow rate remained constant for 12 more min, and was then decreased back to 40% v/v acetonitrile in water. The products were identified by using Agilent 1100 Series multiple wavelength detectors at 280 nm. Methanol washes were run after each sample to zero the baseline. The hydrodynamic size was measured by DLS at 25 °C on a Malvern Zetasizer Nano ZS90 with a He/Ne laser (633 nm) at 173° collecting optics. NP dispersions were prepared at 0.83 and 0.33 mg mL^{-1} using DI water or DMEM containing 10% FBS (both were filtered with a 0.2 μm syringe filter). DI water was used as a negative control (~0 counts). Data were analyzed by Malvern Dispersion Technology Software 4.20. Confocal fluorescence images were collected on a Leica SP8 confocal laser scanning microscope at 590/617 nm excitation/emission. Flow cytometry was conducted in a Beckman Coulter CytoFLEX S cell analyzer (CILS Core Facility, Northeastern University). Analysis was performed using Floreada software. Micro-CT images were collected on a MILabs VECTor^6 CT^{UHR} at the following scanning parameters: 50 keV, 0.21 mA current, 70 s exposure time, and total image time of 3–6 min. All images were set at the same color scale, gray $<-1000, 3000>$.

Conflicts of interest

There are no conflicts to declare.

Data availability

Data regarding synthesis, NMR, LC-MS, HPLC, UV-vis, TEM, TGA, plate reader, confocal microscopy are publicly accessible and available through the UMass Lowell server. Data regarding flow cytometry are available through the Northeastern University server (current institute of the PI). A request for data availability can be made through the corresponding author.

All research data generated have been stored on both local hard drives and on the departmental server, which is backed up daily onto an off-site array of hard drives. In addition, all local hard drives are regularly backed up onto local external hard drives for more expedient recovery in the case of crashes.

Supplementary information (SI): Fig. S1–S23. See DOI: https://doi.org/10.1039/d6ma00016a.

Acknowledgements

This research was funded by the Massachusetts Life Science Center – Women's Health Collaboration Program grant (PI: Gkikas). The content is solely the responsibility of the authors and does not reflect the opinions of the sponsor. The authors would like to express their appreciation to Prof. Mary Rusckowski (UMass Chan Medical School) and Shayesteh Tafazoli (UML) for helping us with Fig. 5 and Fig. 1e respectively, as well as to Wendy Gavin and Dr Anna-Maria Routsi (UML Core Research Facilities). We also thank Prof. Conor Evans and Instructor Emmanuel Roussakis (MGH, Wellman Center for Photomedicine) for using their lab facility for the DLS experiments. Dr Guoxin Rong (CILS Core Facility, Northeastern University) is also appreciated.

References

1 J. R. Harris, M. E. Lippman, U. Veronesi and W. Willett, Breast cancer, *N. Engl. J. Med.*, 1992, **327**, 319–328.
2 J. G. Elmore, K. Armstrong, C. D. Lehman and S. W. Fletcher, Screening for breast cancer, *JAMA*, 2005, **293**, 1245–1256.
3 T. J. Key, P. K. Verkasalo and E. Banks, Epidemiology of breast cancer, *Lancet Oncol.*, 2001, **2**, 133–140.
4 D. Kashyap, *et al.*, Global increase in breast cancer incidence: risk factors and preventive measure, *BioMed Res. Int.*, 2022, **2022**, 1–16.

5 M. Arnold, *et al.*, Current and future burden of breast cancer: Global statistics for 2020 and 2040, *Breast*, 2022, **66**, 15–23.
6 M. G. Marmot, D. G. Altman, D. A. Cameron, J. A. Dewar, S. G. Thompson and M. Wilcox, The benefits and harms of breast cancer screening: an independent review, *Br. J. Cancer*, 2013, **108**, 2205–2240.
7 M. S. Jochelson and M. B. Lobbes, Contrast-enhanced mammography: state of the art, *Radiology*, 2021, **299**, 36–48.
8 C. K. Osborne, M. G. Yochmowitz, W. A. Knight 3rd and W. L. McGuire, The value of estrogen and progesterone receptors in the treatment of breast cancer, *Cancer*, 1980, **46**, 2884–2888.
9 T. Key, P. Appleby, I. Barnes and G. Reeves, Endogenous sex hormones and breast cancer in postmenopausal women: reanalysis of nine prospective studies, *J. Natl. Cancer Inst.*, 2002, **94**, 606–616.
10 P. Toniolo, K. L. Koenig, B. S. Pasternack, S. Banerjee, C. Rosenberg, R. E. Shore, P. Strax and M. Levitz, Reliability of measurements of total, protein-bound, and unbound estradiol in serum, *Cancer Epidemiol., Biomarkers Prev.*, 1994, **3**, 47–50.
11 C. S. Watson, R. A. Alyea, K. A. Cunningham and Y. J. Jeng, Estrogens of multiple classes and their role in mental health disease mechanisms, *Int. J. Womens Health*, 2010, 153–166.
12 D. J. Cahill, P. G. Wardle, C. R. Harlow, L. P. Hunt and M. G. Hull, Expected contribution to serum estradiol from individual ovarian follicles in unstimulated cycles, *Hum. Reprod.*, 2000, **15**, 1909–1912.
13 F. Z. Stanczyka, D. F. Archer and B. R. Bhavnani, Ethinyl estradiol and 17β-estradiol in combined oral contraceptives: pharmacokinetics, pharmacodynamics and risk assessment, *Contraception*, 2013, **87**, 706–727.
14 M. Clemons and P. Goss, Estrogen and the risk of breast cancer, *N. Engl. J. Med.*, 2001, **344**, 276–285.
15 E. R. Prossnitz and M. Barton, The G protein-coupled oestrogen receptor GPER in health and disease: an update, *Nat. Rev. Endocrinol.*, 2023, **19**, 407–424.
16 M. Marino, P. Galluzzo and P. Ascenzi, Estrogen signaling multiple pathways to impact gene transcription, *Curr. Genomics*, 2006, **7**, 497–508.
17 N. Fuentes and P. Silveyra, Estrogen receptor signaling mechanisms, *Adv. Protein Chem. Struct. Biol.*, 2019, **116**, 135–170.
18 I. Paterni, C. Granchi, J. A. Katzenellenbogen and F. Minutolo, Estrogen receptors alpha (ERα) and beta (ERβ): subtype-selective ligands and clinical potential, *Steroids*, 2014, **90**, 13–29.
19 A. W. Brandenberger, M. K. Tee, J. Y. Lee, V. Chao and R. B. Jaffe, Tissue distribution of estrogen receptors alpha (ER-α) and beta (ER-β) mRNA in the midgestational human fetus, *J. Clin. Endocrinol. Metab.*, 1997, **82**, 3509–3512.
20 M. W. Pfaffl, I. G. Lange, A. Daxenberger and H. H. Meyer, Tissue-specific expression pattern of estrogen receptors (ER): quantification of ERα and ERβ mRNA with real-time RT-PCR., *APMIS*, 2001, **109**, 345–355.
21 D. D. Hutson, *et al.*, Estrogen receptor profiles across tissues from male and female rattus norvegicus, *Biol. Sex Differ.*, 2019, **10**, 4.
22 G. Cheng, Z. Weihua, M. Warner and J.-A. Gustafsson, Estrogen receptors ERα and ERβ in proliferation in the rodent mammary gland, *Proc. Natl. Acad. Sci. U. S. A.*, 2004, **101**, 3739–3746.
23 X. Feng, D. Manka, K.-U. Wagner and S. A. Khan, Estrogen receptor-α expression in the mammary epithelium is required for ductal and alveolar morphogenesis in mice, *Proc. Natl. Acad. Sci. U. S. A.*, 2007, **104**, 14718–14723.
24 G. V. Dal, *et al.*, Estrogen receptor subtypes dictate the proliferative nature of the mammary gland, *J. Endocrinol.*, 2018, **237**, 323–336.
25 A. L. Cartaxo, *et al.*, A novel culture method that sustains ERα signaling in human breast cancer tissue microstructures, *J. Exp. Clin. Cancer Res.*, 2020, **39**, 161.
26 P. A. Furth, *et al.*, Overexpression of estrogen receptor α in mammary glands of aging mice Is associated with a proliferative risk signature and generation of estrogen receptor α-positive mammary adenocarcinomas, *Am. J. Pathol.*, 2023, **193**, 103–120.
27 A. M. Gawlik, *et al.*, Late-onset puberty induction by transdermal estrogen in turner syndrome girls – a longitudinal study, *Front. Endocrinol.*, 2018, **9**, 1–8.
28 R. K. Rej, J. E. Thomas, R. K. Acharyya, J. M. Rae and S. Wang, Targeting the estrogen receptor for the treatment of breast cancer: recent advances and challenges, *J. Med.Chem.*, 2023, **66**, 8339–8381.
29 A. Paris, I. Goutal, J. Richard, A. Becret and F. Gueraudu, A comparison of the pharmacokinetic properties of three estradiol esters, *Contraception*, 1980, **21**, 415–424.
30 B. S. Reddy and R. Banerjee, 17β-Estradiol-associated stealth-liposomal delivery of anticancer gene to breast cancer cells, *Angew. Chem., Int. Ed.*, 2005, **44**, 6723–6727.
31 B. Morrow, I. Leav, R. A. Delellis and S. Raam, Use of polyestradiol phosphate and anti-17 beta estradiol antibodies for the localization of estrogen receptors in target tissues: a critique, *Cancer*, 1980, **46**, 2872–2879.
32 S. H. Kim and J. A. Katzenellenbogen, Hormone–PAMAM dendrimer conjugates: polymer dynamics and tether structure affect ligand access to receptors, *Angew. Chem., Int. Ed.*, 2006, **45**, 7243–7248.
33 C.-Y. Tsai, C.-W. Li, J.-R. Li, B.-H. Jang and S.-H. Chen, Steroid probes conjugated with protein-protected gold nanocluster: specific and rapid fluorescence imaging of steroid receptors in target cells, *J. Fluoresc.*, 2016, **26**, 1239–1248.
34 C. Tang, Y. Du, Q. Liang, Z. Cheng and J. Tian, A novel estrogen receptor α-targeted near-infrared fluorescent probe for in vivo detection of breast tumor, *Mol. Pharmaceutics*, 2018, **15**, 4702–4709.
35 B. Mamnoon, L. Feng, J. Froberg, Y. Choi, V. Sathish and S. Mallik, Hypoxia-responsive, polymeric nanocarriers for targeted drug delivery to estrogen receptor-positive breast cancer cell spheroids, *Mol. Pharmaceutics*, 2020, **17**, 4312–4322.

36 D. M. Tanenbaum, Y. Wang, S. P. Williams and P. B. Sigler, Crystallographic comparison of the estrogen and progesterone receptor's ligand binding domains, *Proc. Natl. Acad. Sci. U. S. A.*, 1998, **95**, 5998–6003.

37 K. J. Pawlak and J. P. Wiebe, Regulation of estrogen receptor (ER) levels in MCF-7 cells by progesterone metabolites, *J. Steroid Biochem. Mol. Biol.*, 2007, **107**, 172–179.

38 A. Kasid, J. S. Strobl, K. Huff, G. L. Greene and M. E. Lippman, A novel nuclear form of estradiol receptor in MCF-7 human breast cancer cells, *Science*, 1987, **225**, 4667.

39 R. Jakesz, C. A. Smith, S. Aitken, K. Huff, W. Schuette, S. Shackney and M. Lippman, Influence of cell proliferation and cell cycle phase on expression of estrogen receptor in MCF-7 breast cancer cells, *Cancer Res.*, 1984, **44**, 619–625.

40 Y. Zhou, L. Yan, T. Maji, G. Lévêque, M. Gkikas and G. Fytas, Harnessing polymer grafting to control the shape of plasmonic nanoparticles, *J. Appl. Phys.*, 2020, **127**, 074302.

41 K. Ramesh, A. Truong, Y. Wang, M. Rusckowski and M. Gkikas, Ligand-Specific nano-contrast agents promote enhanced breast cancer CT detection at 0.5 mg Au, *Int. J. Mol. Sci.*, 2022, **23**, 9926.

42 T. Farrokhi and M. Gkikas, NanoGraphene clot: a new fibrinogen-mimic hemostatic material, *ACS Appl. Mater. Interfaces*, 2024, **16**, 34783–34797.

43 V. P. Torchilin and V. S. Trubetskoy, Which polymers can make nanoparticulate drug carriers long-circulating?, *Adv. Drug Delivery Rev.*, 1995, **16**, 141–155.

44 M. J. Mitcell, M. M. Billingsley, R. M. Haley, M. E. Wechsler, N. A. Peppas and R. Langer, Engineering precision nanoparticles for drug delivery, *Nat. Rev. Drug Discovery*, 2021, **20**, 101–124.

45 E. Papini, R. Tavano and F. Mancin, Opsonins and dysopsonins of nanoparticles: facts, concepts, and methodological guidelines, *Front. Immunol.*, 2020, **11**, 567365.

46 Q.-Y. Cai, S. H. Kim, K. S. Choi, S. Y. Kim, S. J. Byun, K. W. Kim, S. H. Park, S. K. Juhng and K.-H. Yoon, Colloidal gold nanoparticles as a blood-pool contrast agent for X-ray computed tomography in Mice, *Investig. Radiol.*, 2007, **42**, 797–806.

47 J. R. Ashton, D. P. Clark, E. J. Moding, K. Ghaghada, D. G. Kirch, J. L. West and C. T. Badea, Dual-energy micro-CT functional imaging of primary lung cancer in mice using gold and iodine nanoparticle contrast agents: a validation study, *PLoS One*, 2014, **9**, e88129.

48 K. Smith, M. Getzin, J. J. Garfield, S. Suvarnapathaki, G. Camci-Unal, G. Wang and M. Gkikas, Nanophosphor-based contrast agents for spectral X-ray imaging, *Nanomaterials*, 2019, **9**, 1092.

49 I. Chatzaki and M. Gkikas, Osteoarthritis/inflammation *in vitro* detection using a hyaluronate-coated Au nano contrast probe, *ACS Appl. Nano Mater.*, 2024, **7**, 10194–10204.

50 J. F. Hainfeld, M. J. O'Connor, F. A. Dilmanian, D. N. Slatkin, D. J. Adams and H. M. Smilowitz, Micro-CT enables microlocalisation and quantification of her2-targeted gold nanoparticles within tumour regions, *Br. J. Radiol.*, 2011, **84**, 526–533.

51 T. Reuveni, M. Motiei, Z. Romman, A. Popovtzer and R. Popovtzer, Targeted gold nanoparticles enable molecular CT imaging of cancer: an *in vivo* study, *Int. J. Nanomed.*, 2011, **6**, 2859–2864.

52 R. Meir and R. Popovtzer, Cell tracking using gold nanoparticles and computed tomography imaging, *Wiley Interdiscip. Rev.: Nanomed. Nanobiotechnol.*, 2018, e1480.

53 M. Bouché, J. C. Hsu, Y. C. Dong, J. Kim, K. Taing and D. P. Cormode, Recent advances in molecular imaging with gold nanoparticles, *Bioconjugate Chem.*, 2019, **31**, 303–314.

54 L. M. Nieves, *et al.*, Renally excretable silver telluride nanoparticles as contrast agents for X-ray imaging, *ACS Appl. Mater. Interfaces*, 2022, **14**, 34354–34364.

55 P. M. Peiris, *et al.*, Vascular targeting of a gold nanoparticle to breast cancer metastasis, *J. Pharm. Sci.*, 2015, **104**, 2600–2610.

56 S. V. R. Jonnalagadda, A. J. Gerace, K. Thai, J. Johnson, K. Tsimenidis, J. M. Jakubowski, C. Shen, K. J. Henderson, P. Tamamis and M. Gkikas, Amyloid peptide scaffolds coordinate with Alzheimer's disease drugs, *J. Phys. Chem. B*, 2020, **124**, 487–503.

57 M. Gkikas, S. J. Haataja, J. Ruokolainen, O. Ikkala, H. Iatrou and N. Houbenov, Complexation-driven mutarotation in poly(L-proline) block copolypeptides, *Biomacromolecules*, 2015, **16**, 3686–3693.

58 H. latrou, K. Dimas, M. Gkikas, C. Tsimplouli and S. Sofianopoulou, Polymersomes from polypeptide containing triblock co- and terpolymers for drug delivery against pancreatic cancer: Asymmetry of the external hydrophilic blocks, *Macromol. Biosci.*, 2014, **9**, 1222–1238.

59 H. S. Yoo and T. G. Park, Biodegradable polymeric micelles composed of doxorubicin conjugated PLGA-PEG block copolymer, *J. Controlled Release*, 2001, **70**, 63–70.